International Journal of Latest Research in Engineering and Management" (IJLREM)
ISSN: 2456-0766
www.ijlrem.org ǁ Volume 04 Issue 08 ǁ August 2020 ǁ PP 01-16

MECHANICAL RESPONSE AND FRACTURE BEHAVIOR OF A HIGH-PERFORMANCE STAINLESS STEEL: INFLUENCE OF MICROSTRUCTURE

Anil Patnaik[1**], K. Dheeraj[1#], K. Manigandan[2*]and T. S. Srivatsan[2**]
[1] *Department of Civil Engineering*
The University of Akron
Akron, OHIO 44325, USA
[2] *Department of Mechanical Engineering*
The University of Akron
Akron, Ohio 44325, USA
Graduate Student; * Associate Professor; ** Professor

Abstract: Through the years' stainless steels have gained increased attention for use as a potentially viable reinforcement in concrete structure that are often chosen for use in a spectrum of applications in the domains spanning civil construction, transportation and infrastructure development. This is essentially because of the superior resistance of stainless steel and resultant concrete structure to environment-induced degradation, which is referred to in the real-world as 'corrosion'. In this paper, the specific role of composition of the chosen stainless steel in synergism with secondary processing, i.e., heat treatment, in influencing microstructural development through the formation and presence of phases and other intrinsic microstructural features is highlighted. The conjoint influence of intrinsic microstructural features and nature of loading on hardness, strength, tensile response and cyclic fatigue response is neatly presented and appropriately discussed. The mutually interactive influences of intrinsic microstructural effects and nature of loading, i.e., quasi-static and cyclic, on macroscopic fracture behavior and intrinsic mechanisms governing fracture at the fine microscopic level is presented and briefly discussed.

Keywords: Stainless steel, composition, processing, microstructure, mechanical response, fracture behavior

1. Introduction

The gathering of metals based entirely on compositions, which includes the family of stainless steels, initiated way back in 1913 in the city of Sheffield, England. Harry Brierley [1] was both attempting and studying various combinations and observed very much in conformance with his expectations that the specimens while being cut during one of these trials failed to show evidence of "gross" rusting and were concurrently found hard to carve. Upon further exploration of this curious metal he noticed that it contained around 13 percent chromium [Cr] [2]. This led the metal to be classified as "stainless steel". This unique property offered by stainless steel led to its selection and use for purposes of cutlery. It was cutlery made from stainless steels that eventually made the company based in Sheffield (England) very popular. At around the same time sustained advances were being made in France in the domain spanning steels, which culminated in the development and emergence of austenitic stainless steels [3-5].

As of this date, the overall utilization of stainless steel for a wide spectrum of applications is continuing to grow particularly in industries that offer a multitude of products for use in both performance-critical and non-performance critical applications [1,3, 7, 9]. There is an increased interest being shown by the civil construction industry where stainless steel is being frequently chosen and used for its alluring appearance, corrosion resistance, low maintenance cost coupled with improved quality.

Essentially, stainless steels can be categorized as iron-based compounds that contain around 10.5 to 11.0 pct. chromium. This results in the formation and presence of a defensive self-mending oxide film, which is the primary motivation behind why this class of steels has been given the trademark "stainlessness". The capacity of the thin oxide film, or layer, to mend itself suggests that this steel is safe against environment-induced degradation, also referred to as corrosion, regardless of the nature and severity of the surrounding environment and the extent

and depth of corrosion of the surface. However, this is not the situation when both carbon steels and low alloy steels are shielded from corrosion using the following two techniques: (i) metallic coatings made of zinc or cadmium, and (ii) the use of natural coating, such as, paint [6].

To defeat the issue of a gradually corroding carbon steel and its concomitant influence on the overall structure, that often culminates in structural problems and the need for expensive repairs, which if not done timely often culminates in failure of the concrete structure, we can either change the environment to which the civil structure is exposed to or alternatively change the material. The presence of salt in the environment, such as salt on the roads during the winter months, contributes in an observable manner to saturating and interacting with the concrete structure and there can be little expectation of a change in the environment. Similarly, in a marine environment the salt content is not likely to change. Consequently, reinforcing the concrete structure with stainless steel, as opposed to carbon steel or alloy steel, is an economically viable and affordable method to enhance the overall durability and life of a concrete structure. Likewise, the prudent use of stainless steels does offer the benefit of cost, which is acknowledged by the following [9]:

(1) A gradual minimization in use of the following: (i) rebar coatings, (ii) corrosion inhibitors, (iii) concrete sealers, (iv) membranes, and (v) thick concrete overlay, and
(2) Financial related misfortune arising because of both traffic and commercial upsets.

Stainless steel is often preferred and chosen primarily because it offers good corrosion resistance, acceptable strength coupled with the capability for enhanced service life. The increase in cost arising from the selection and use of stainless steel as reinforcing bars in concrete usually ranges from one to three percent by volume depending on both complexity and cost of the structure. Furthermore, stainless steels offer either the same or higher strength than both carbon steel and even the family of alloy steels. The chosen stainless-steel compositions often offer a healthy combination of natural corrosion resistance, and improved resistance to: (i) pitting corrosion, (ii) crevice corrosion, and (iii) stress corrosion cracking.

2. Material and Sample Preparation

2.1 Material

The material chosen for this study was the Duplex Stainless Steel 2304 provided by Salit Specialty Rebar [Niagara Falls, New York, USA]. The nominal chemical composition of this steel is given in **Table 1.** Presence of carbon provides both solid solutions strengthening and hardenability through the formation and presence of alloy carbides in the microstructure. The alloy carbide particles contribute to enhancing strength at both room temperature and elevated temperature while concurrently enhancing the overall high temperature resistance and creep strength of a predominantly ferrite matrix. This steel is rich in chromium content and adequate amount of nickel (Ni) with minimal amount of molybdenum (Mo). The presence of chromium [Cr], assists in the formation and presence of carbide particles, which contributes to enhancing strength of the steel matrix. However, the presence and distribution of carbide particles in the microstructure is often detrimental to both fracture toughness, or impact resistance, and cyclic fatigue resistance as a direct consequence of increasing the number of potential sites for the early initiation of fine microscopic cracks. Presence of nickel [Ni] facilitates in lowering the transition temperature while simultaneously enhancing toughness and stabilizing the austenite phase that is present in the microstructure [9]. The presence of molybdenum (Mo) plays a role in refining the grain size while concurrently aiding in the formation and presence of molybdenum carbides, which are dispersed through the microstructure. The low nickel and high chromium content plus a duplex microstructure do give this stainless-steel improved stress corrosion resistance and fracture toughness properties compared to the popular grades of stainless steel 304 and 316 [1,7,9].

Table 1. Nominal chemical composition of Stainless Steel 2304
(in weight percent)

Material	Fe	Cr	Ni	Mn	Si	Cu	Mo	N
Stainless Steel (2304)	**70.55**	**22.84**	**3.64**	**1.72**	**0.46**	**0.31**	**0.26**	**0.17**

2.2 Secondary Processing

This stainless steel was hot rolled at 1000ºC. After hot rolling this stainless steel was annealed at 950ºC with the prime purpose of utilizing the benefits of annealing and concurrently restoring the corrosion resistance properties and mechanical properties. As a final step in manufacturing this stainless steel was subject to "pickling". Pickling aids in removal of the traces of any oxide(s) present on the surface while concurrently aiding in the removal of impurities, such as, (i) stains, (ii) inorganic contaminants, (iii) rust or scale. A solution called 'pickle liquor', containing an acid, was used to ensure complete removal of any and all impurities on the surface. The technique of pickling is an important step in the manufacture of stainless steel and prior to enabling the steel for use in real-world applications.

2.3 Preparation of Test Specimen

Full length rebar's of the duplex stainless steel are customarily chosen for use as the reinforcement for reinforced concrete structures. The rebar was cut into small pieces, each of size 2.5 inches. The cut samples were then precision machined in conformance with standards specified in ASTM E-8 [10]. A schematic of the machined test specimen is shown in **Figure 1**.

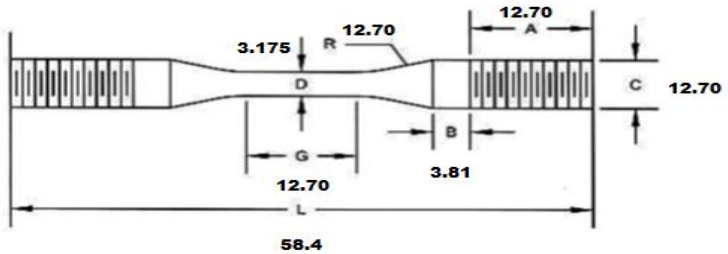

Figure 1. Schematic of the cylindrical test specimen used for mechanical testing.

3. Experimental Procedures

3.1 Characterization of Initial Microstructure

An initial characterization of the microstructure of the as-provided steel was done using a low magnification optical microscope. Samples of the required size were cut from the as-received stainless-steel material and mounted in epoxy. The mounted samples were then prepared very much in conformance with the standard procedures used for metallographic preparation of metal samples. This involved systematic coarse polish using progressively finer grades of silicon carbide (SiC) impregnated emery paper using copious amount of water both as coolant and lubricant. This was followed by fine polishing using 5-micron alumina-based polishing compound and 1-micron alumina-based polishing compound suspended in distilled water as the lubricant. The as-polished samples were then etched using a reagent. Etching helps in: (a) revealing the grain boundaries, essentially the high angle grain boundaries, (b) the morphology of the grains, and (iii) other fine intrinsic features, of observable size, dispersed through the microstructure. The etchant used is a solution mixture of 16.67 pct. hydrochloric acid (HCl) and 83.33 pct. distilled water (H_2O). In other words, 200 ml of HCl for 1000 ml of H_2O [7,9]. The polished and etched surface of the steel samples were observed in an optical microscope, at low magnifications, and photographed using standard bright field illumination technique.

3.2 Hardness testing

Hardness of a material is a mechanical property defined as the resistance offered by the material to indentation i.e., permanent deformation and cracking [2,11].

3.2.1 Microhardness tests

The Vickers microhardness (Hv) of the duplex stainless steel 2304 samples was measured using a microhardness test machine [Model: Wilson Tukon 2100B]. The diamond indenter has a square base and pyramidal geometry with an included angle of 136 degrees. The machine makes an indent, or impression, on the sample surface whose size of the diagonal was precision measured using a low magnification optical microscope. The indentation load used was 0.75kgf. Use of lower loads with specific reference to high strength steels and the family of stainless steels was not considered since it can cause problems arising from the following: (i) dependence of hardness on indentation load, and (ii) measurement uncertainty arising from very small size of the indent. The Vickers hardness number (Hv) is expressed as the ratio of the applied load to surface area of indent. To minimize uncertainties arising from both measurement and cracking and their mutually interactive influences an indentation load of 0.5kgf for a dwell time of 15 seconds was chosen and used. At least four indents in each direction, i.e., longitudinal (L) and transverse (T), were made on the polished surface of the chosen stainless-steel sample and the result is reported as an average value in units of kg/mm^2.

3.2.2 Macro Hardness tests

The Rockwell hardness (R_B) test is a static indentation test that is quite like the Brinell indentation test. It differs from the Brinell test in that it measures the depth of indentation following the application of an initial load of 98.1 N. This is followed by the continued application of an additional load. The Rockwell hardness number is directly read (in units of 0.002mm) from the dial gauge, which is attached to the Rockwell machine. For the stainless-steel samples used in this study an indentation load of 150kgf, using 120-degree diamond cone for a dwell time of 10 seconds was used and the hardness value read on the "B" scale [2,11]. The indents were made edge-to-edge across the polished surface of the sample of stainless steel, and the result is reported as an average value in units of kg/mm^2 [2,11].

3.3 Mechanical Testing

3.3.1 Tensile tests

Uniaxial tests were performed, up until failure of the test specimen, on a closed-loop servo-hydraulic mechanical test machine [Model: INSTRON-8500 plus], using a 100 KN load cell. The tests were performed both at room temperature (80 ^{0}F) and at an elevated temperature (400 ^{0}F) in an environment of laboratory air [Relative Humidity of 55 percent]. The test samples of the stainless steel were deformed at a constant strain rate of 0.0001/sec. An axial 12.5-mm gage length clip-on extensometer was attached to the test specimen using: (i) rubber bands for the tests at room temperature (80^{o}F), and (ii) steel springs for the tests at elevated temperature (400^{o}F), to provide a precise measure of the strain experienced by the test specimen during uniaxial loading and resultant stretching. The stress and strain measurements, parallel to the load line, were recorded on a PC–based data acquisition system (DAS).

3.3.2 Cyclic Stress Controlled or High Cycle Fatigue Test

The cyclic stress–amplitude controlled high cycle fatigue (HCF) tests were performed utilizing a sinusoidal waveform and a stress ratio [R = Minimum stress/Maximum stress] of - 1. The test specimens were cyclically deformed at a frequency of 5 Hz. At the chosen stress ratio (R) of -1, the cyclic fatigue tests were conducted over a range of stress amplitudes to establish the variation of maximum stress ($\sigma_{maximum}$) with cyclic fatigue life (N_F) [12-15]. The stress amplitude-controlled fatigue tests were performed at both ambient (room) temperature (80^{o}F) and chosen elevated temperature. The elevated temperature chosen in this study was 400^{o}F. A thermocouple was used to measure and control temperature of the test specimen that was placed within an environmental chamber. At the chosen stress ratio of -1, the fatigue tests were conducted over a range of stress amplitudes ($\sigma_{amplitude}$) to establish the following:

a. The variation of ratio of maximum stress ($\sigma_{maximum}$) with fatigue life (N_f).
b. The variation of percentage of yield stress (σ_{max} / $\sigma_{yield\ stress}$) with fatigue life (N_f).
c. Variation of maximum elastic strain [$\sigma_{maximum}$ / E] with fatigue life (N_f)

3.4 Failure-Damage analysis

Fracture surfaces of the stainless-steel samples that were deformed and failed, both in tension and cyclic fatigue, were examined in a scanning electron microscope (SEM). This was done to help establish the macroscopic fracture mode while concurrently characterizing and/or determining the fine-scale features on the fracture surface to help establish the microscopic mechanisms governing fracture during both tensile loading and cyclic loading.

4. Results and Discussions

4.1 Initial Microstructure

The microstructure of the starting material is an important factor to be considered in a study aimed at quantifying its properties. Properties spanning tensile strength, fracture strain or ductility, cyclic fatigue resistance and resultant fracture behavior can be rationalized for purpose of its selection and use in a desired application. An optical micrograph of the longitudinal (L) section of the as provided stainless steel 2304 is shown in the **Figure 2 (a).** An optical micrograph of the transverse (T) section of the same stainless steel 2304 specimen is shown in **Figure 2 (b).** The longitudinal (L) section reveals a mixture of light and dark regions. The light color region, or island, can be categorized as pockets of ferrite (pure iron), while the darker or gray color region is a mixture of very fine pearlite and austenite.

Also, the longitudinal (L) section of the sample revealed an absence of coarse second-phase particles at the allowable magnifications of the light optical microscope. The transverse (T) section of the stainless steel 2304 revealed a healthy mixture of very fine grains. The light color region, or island, represents ferrite (or pure iron), while the darker region represents a combination of pearlite and austenite. Overall, the microstructure of this stainless steel is stable when compared one-on-one to molybdenum-containing stainless steel. The intermetallic phases, if any, are fine, small and dispersed through the microstructure and not easily resolvable at the allowable magnifications of the light microscope.

The presence and distribution of these micro-constituents is governed by a synergism of composition and primary processing technique used to manufacture the starting material, i.e., as provided stainless steel, and does exert an influence on “local” hardness, global tensile response, cyclic fatigue resistance and overall fracture behavior.

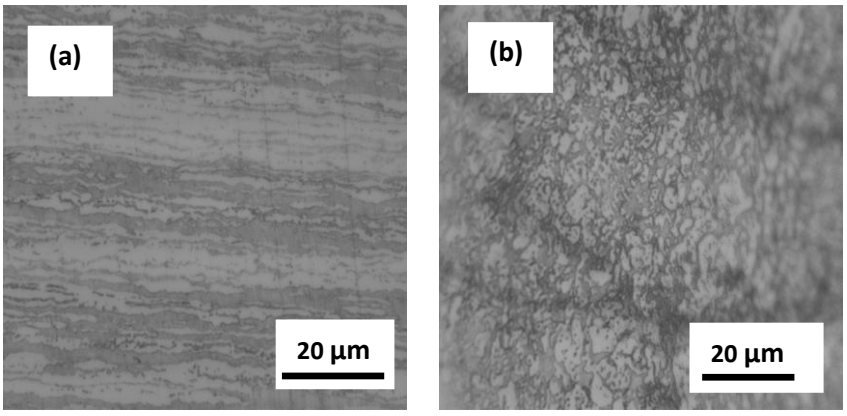

Figure 2. Optical micrograph showing key micro-constituents in the duplex stainless steel 2304: (a) Longitudinal (L), and (b) Transverse (T)

4.2 Hardness

Hardness is defined as the amount of resistance a material provides to permanent deformation by way of indentation [2, 11]. It is the easiest method for quantifying certain mechanical properties of a material.

4.2.1 Microhardness measurement

Microhardness testing can be defined as indentation hardness testing that involves forcing a diamond indenter having a specific geometry onto the surface of the test material at varying loads depending upon hardness of the material that is being indented. A few trials were made to gather a detailed set of readings over both the longitudinal (L) and transverse(T) sections of the sample while concurrently establishing the variation. The microhardness measurements provide a measure of the net strengthening effect arising from a combination of composition, primary processing used, and secondary processing, if any, that was used to make available the starting material, and the weakening effect arising from the presence and distribution of processing-related defects or artifacts. The presence of processing-related defects, such as: (a) fine microscopic pores, (b) fine microscopic voids, and (c) fine microscopic cracks, when intercepted by the pyramidal indenter does often result in a net decrease in value of the measured microhardness of the stainless-steel sample. The microhardness values of the duplex stainless steel 2304 are summarized in **Table 2**. The indentation load used was 1 kgf for a dwell time of 15 seconds. The average value of microhardness was found to be 514 kg/mm^2.

Table 2. A compilation of results of the Vickers micro-hardness test

Material		**Trial # 1**	**Trial # 2**	**Trial # 3**	**Trial # 4**	**Average Hardness Kg / mm^2**
SS 2304	D1 (µM)	64.91	60.81	58.19	62.88	
	D2 (µM)	56.07	64.91	59.75	53.91	
	Average (µM)	60.49	62.86	58.97	58.40	
	Load (Kg)	1	1	1	1	
	Duration (Seconds)	15	15	15	15	
	Microhardness (Kg/mm^2)	507	469	534	544	**514.0**

4.2.2 Macro-hardness measurement

The macro-hardness values, summarized in **Table 3**, were taken using the Rockwell B scale across the length of a sample of stainless steel 2304 and range from 68.90 kg/mm^2 to 76.63 kg/mm^2 with an average value of 74.17 kg/mm^2.

Table 3. A compilation of the results obtained from Macro-hardness test

Material		**Trial # 1**	**Trial # 2**	**Trial # 3**	**Trial # 4**	**Average Hardness**
SS 2304	R_B	93	97	96	97	95.75
	Hardness (ksi)	98	109	106	109	105.5
	Hardness (kg/mm^2)	68.90	76.63	74.53	76.63	**74.17**

4.3 Tensile Response: Influence of temperature

4.3.1 Properties

Tensile properties of the chosen steel (Duplex stainless steel 2304), at both ambient temperature (80^0F) and elevated temperature (400^0F) are summarized in **Table4**.Results reported are the mean values based on duplicate tests.

(i) The elastic modulus of stainless steel 2304 was 242 GPa at room temperature (80^o F) and 222 MPa at the elevated temperature (400^oF), a nine percent decrease in the elastic modulus (E) with an increase in test temperature.

(ii) Yield strength (σ_{ys}) of the stainless steel at room temperature (80^o F) was 648 MPa and at the elevated temperature (400^o F) 530 MPa; a noticeable decrease in strength of twenty percent with an increase in test temperature from 80^oF to 400^o F.

(iii) The ultimate tensile strength (σ_{UTS}) at room temperature (80^oF) was 808 MPa and718 MPa at the elevated temperature (400^o F), an observable decrease in strength by 11 percent due to the increase in test temperature from 80^oF to 400^oF.

(iv) The ductility quantified by elongation-to-failure (ε_f) was 48.0 pct. at room temperature (80^o F) and 40.0 pct. at the elevated temperature (400^o F).

Table 4. A compilation of uniaxial tensile properties of stainless steel 2304 at room temperature (80^0F) and elevated temperature ($400\ ^0$F).
[Results are the mean values based on duplicate tests]

Temperature	Elastic Modulus [GPa]	Yield Strength [MPa]	Tensile Strength [MPa]	Ductility [%]
27^{o}C (80 F)	242	648	808	48.0
205^{o}C (400 F)	222	530	718	40.0

4.3.2 Tensile fracture behavior

Tensile fracture surfaces of the chosen stainless steel 2304 at both ambient temperature (80^o F) and elevated temperature (400^o F) were examined in a scanning electron microscope (SEM) to provide useful information pertaining to the specific role of intrinsic microstructural constituents and features on strength, ductility and fracture properties of the chosen stainless steel. Representative fractographs for the two chosen orientations [longitudinal (L) and transverse (T)] are shown in **Figure 3** and **Figure 4**.

4.3.2.1 Tensile fracture at ambient temperature [80^o F]:

Scanning electron micrographs of the tensile fracture surface of the sample tested at ambient temperature (80^O F) revealed macroscopic fracture to occur by the characteristic "cup and cone" type of separation, which is an indication of ductile fracture. The overall morphology is shown in **Figure 3 (a)**. High magnification observation of the fracture surface in the region of damage initiation revealed an array of fine microscopic voids and dimples of varying size and shape. These features are clearly indicative of the "locally" operating ductile failure mechanisms. This can be seen in **Figure 3 (b)**. The fine microscopic cracks were surrounded by an observable population of microscopic voids and dimples, as shown in **Figure 3 (c).** These fine features on the tensile fracture surface are indicative of "locally" operating brittle and ductile failure mechanisms. The region of overload revealed a sizeable population of microscopic voids inter-dispersed with shallow dimples **(Figure 3 (d)),** which is indicative of the occurrence of 'locally' ductile failure mechanism.

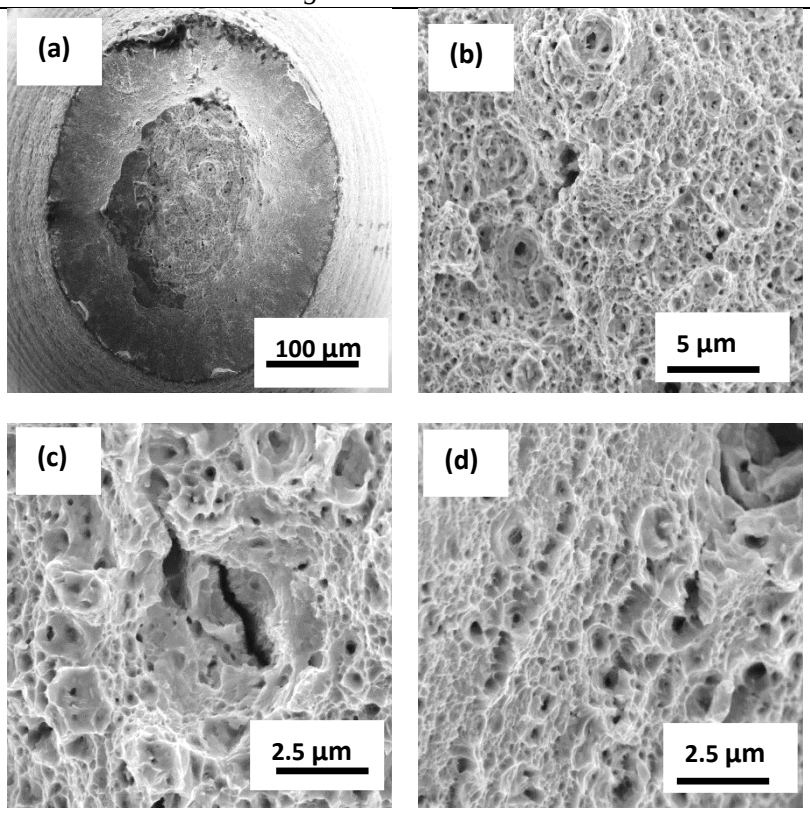

Figure 3. Scanning electron micrographs of the tensile fracture surface of stainless steel 2304 deformed at room temperature (80°F), showing:
(a) Overall morphology of failure
(b) Region of early damage initiation inlaid with an array of fine microscopic voids and dimples, features indicative of locally ductile failure mechanisms.
(c) Fine microscopic cracks surrounded by microscopic voids and dimples indicative of locally brittle and ductile failure mechanisms.
(d) Microscopic voids inter-dispersed with shallow dimples in the region of overload indicative of 'locally' ductile failure mechanism.

4.3.2.2 Tensile fracture at the elevated temperature (400° F).

Scanning electron microscopy (SEM) observations of the sample of stainless steel 2304 deformed in tension at the chosen elevated temperature [400° F], revealed the following observations. The overall morphology of failure was primarily ductile as shown in **Figure 4 (a)** and was essentially "cup and cone" type separation indicative of globally ductile failure. Observation of the fracture surface at higher magnifications revealed many features. These features are a combination of: (i) dimples of varying size and shape, (ii) isolated microscopic voids, and (iii) an array of fine microscopic cracks and macroscopic cracks (**Figure 4(b)**). These features are clearly indicative of both brittle and ductile failure mechanisms acting at the fine microscopic level. A sizeable population of fine microscopic voids inter-dispersed with dimples is shown in **Figure 4 (c)**. These features are indicative of 'locally' dominant ductile failure mechanism. The overload fracture surface revealed a population of voids of varying size in combination with an observable population of dimples covering the fracture surface (**Figure 4 (d**)). These features are indicative of the occurrence of "locally" dominant ductile failure mechanisms.

4.4 Cyclic stress-controlled fatigue

4.4.1 Ambient temperature (80° F)

The results of the axial stress-controlled fatigue tests, at ambient temperature (27^0C), are as follows.

(a) The first specimen was tested at 75 pct. of the yield stress (σ_{ys}), which was a maximum stress of 486 MPa and the amplitude of load being 3.846 K-N. The specimen failed in the gage section following 6,600 cycles.

(b) The second specimen was tested at 70 pct. of the yield stress (σ_{ys}), i.e., at a maximum stress of 454 MPa and an amplitude of loading being 3.590 K-N. This specimen failed in the gage section after 35,000 cycles.

(c) The third specimen was tested at 60 pct. of the yield stress (σ_{ys}), i.e., at a maximum stress of 389 MPa and an amplitude of load being 3.077 K-N, resulting in a fatigue life of 96,000 cycles, with failure occurring at the gage section.

(d) The fourth specimen was tested at 55 pct. of the yield stress, i.e., at a maximum stress of 356 MPa with an amplitude of 2.821 K-N and failure occurred after 883,000 cycles. This specimen too failed in the gage section.

(e) The final sample, at ambient temperature, was tested at 50 pct. of the yield stress (σ_{ys}). For this specimen the maximum stress was 324 MPa with an amplitude of load was 2.564K-N. For this specimen failure did not occur even after one million (1,000,000) cycles.

The test results obtained at ambient temperature are plotted to exemplify the variation of maximum stress ($\sigma_{maximum}$) with fatigue life, or cycles-to-failure, (N_f) and shown in **Figure 5.**

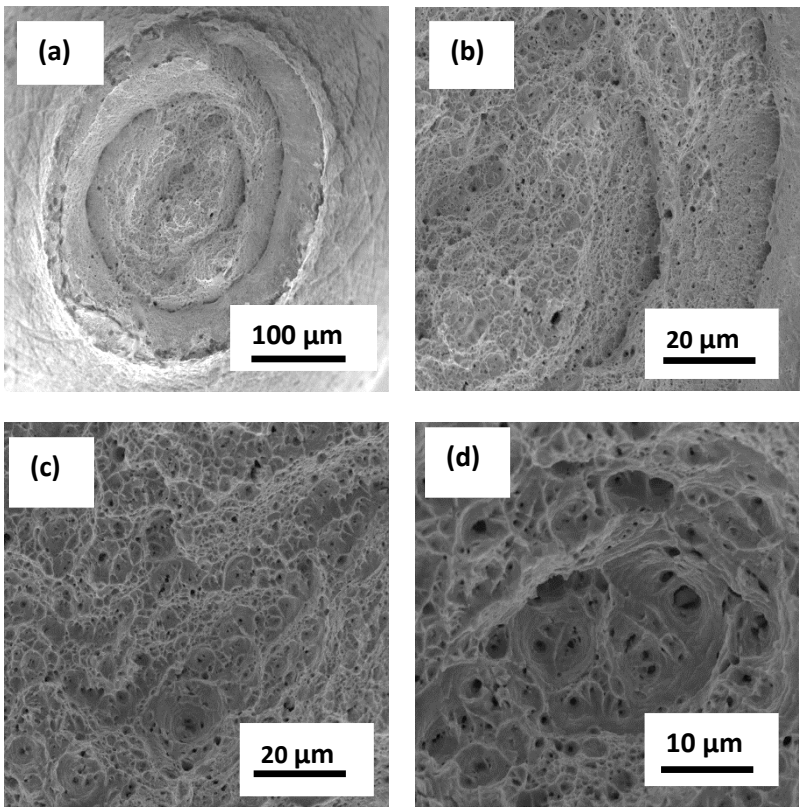

Figure 4. Scanning electron micrographs of the sample of stainless steel 2304 deformed in tension at an elevated temperature of 400ºF, showing:
(a) Overall morphology of failure revealing cup and cone morphology
(b) High magnification observation of (a) revealing dimples of varying size, isolated microscopic voids and macroscopic crack; features indicative of both brittle and ductile failure mechanism.
(c) Population of microscopic voids inter-dispersed with dimples, features indicative of 'locally' ductile failure mechanism.
(d) A population of voids of varying size and dimples covering the overload fracture surface.

4.4.2 Elevated temperature (400ºF)

Results of the axial stress-controlled fatigue tests, at the chosen elevated temperature (400^0 F), are as follows. Similar to observation at the ambient temperature (80^o F), even at the elevated test temperature (400^0 F), five test specimens were cyclically deformed over a range of stress amplitudes.

(a) The first specimen was tested at 72.5 pct. of the yield stress (σ_{ys}), i.e., at a maximum stress of 383.98 MPa and an amplitude of 3.038 K-N. This specimen failed at the gage section after 11,052 cycles.

(b) The second specimen was tested at 65 pct. of the yield stress (σ_{ys}), i.e., at a maximum stress of 344.26 MPa and an amplitude of 2.724 K-N. This specimen failed at the gage section after 11,351 cycles.

(c) The third specimen was tested at 60 pct. of the yield stress (σ_{ys}), i.e., at a maximum stress of 317.78 MPa and an amplitude of load being 2.515 K-N. Following 48,839 cycles, this specimen experienced failure at the gage section.

(d) The fourth specimen was tested at 55 pct. of the yield stress (σ_{ys}), i.e., at a maximum stress of 291.29MPa, and an amplitude of load being 2.305 K-N. After 87446 cycles, this specimen experienced failure at the gage section.

(e) The final sample was tested at 50 pct. of the yield stress (σ_{ys}), i.e., at a maximum stress of 269 MPa. The amplitude of load was 2.095 K-N. This sample did not fail even after one million (1,000,000) cycles.

The test results obtained at the elevated temperature (400^0F) are plotted as the variation of maximum stress ($\sigma_{maximum}$) with fatigue life (cycles-to-failure) and compared with test results obtained at the ambient (room temperature). This is also shown in **Figure 5**.

Variation of percentage of yield stress [$\sigma_{maximum} / \sigma_{yield\ strength}$] with cyclic fatigue life (N_f) is shown in **Figure 6**. This figure reveals a degradation in high cycle fatigue life (N_f) with an increase in test temperature at all values of applied maximum stress or percentage of yield stress. The degradation is as high as 100 pct.

4.5 Cyclic fracture behavior

A comprehensive examination of the fracture surfaces of the cyclically deformed and failed test specimens were done using a scanning electron microscope (SEM) [Model: FEI Quanta 200] over a range of allowable magnifications. Low magnification observations were used to identify regions specific to: (i) fatigue-related failure, and (ii) final fracture (overload). Gradually higher magnifications were used to observe key features on the fatigue fracture surfaces in the regions specific to fatigue failure and overload with the prime purpose of identifying the following.

(a) Location of microscopic crack initiation.
(b) Nature, extent and severity of early microscopic and macroscopic crack growth through the microstructure, and
(c) Other fine scale features present on the fracture surface.

Representative fracture features are shown for the test specimens that were cyclically deformed, at ambient temperature (80° F) [**Figure 7** and **Figure 8**] and elevated temperature (400° F) [**Figure 9** and **Figure** 10], at:

(i) A high value of maximum stress and resultant short fatigue life (N_f), and at
(ii) A low value of maximum stress and resultant enhanced fatigue life (N_f).

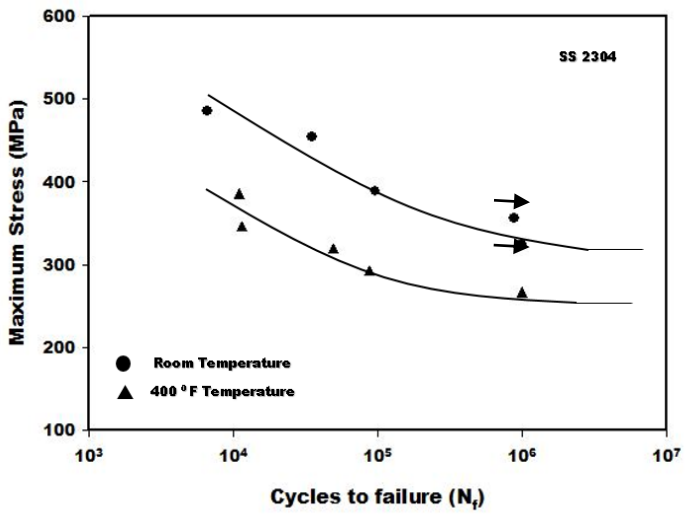

Figure 5. A comparison of the variation of maximum stress (σ_{max}) with fatigue life or cycles-to- failure (N_f) for the duplex stainless steel 2304 at a stress ratio of -1.

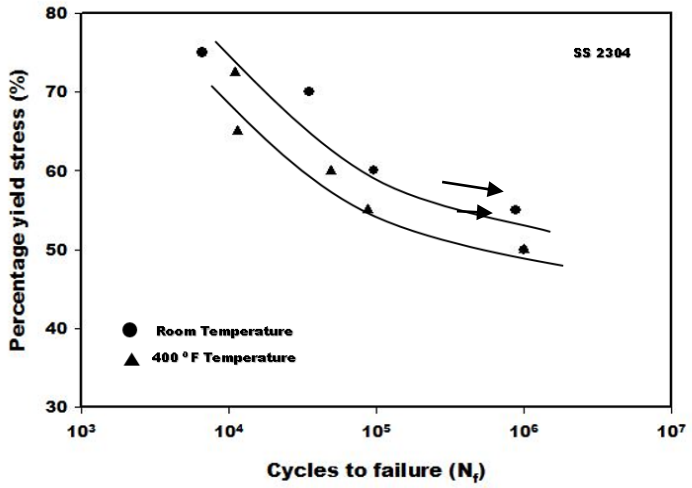

Figure 6. A comparison of the influence of test temperature on variation of percentage of yield stress ($\sigma_{maximum}$) with fatigue life (N_f) for the duplex stainless steel 2304 at a stress ratio of -1.

4.5.1 At ambient (room) temperature (80° F)

Scanning electron micrographs of the sample of stainless steel 2304 cyclically deformed at this temperature (80 ° F) at a maximum stress of 389 MPa and a resultant fatigue life of 96,000 cycles are shown in **Figure 7**. The overall morphology of failure is as shown in **Figure 7 (a).** This micrograph clearly reveals the regions of: (a) crack initiation, (b) stable crack growth, and (c) overload. A high magnification observation of the region of crack initiation is shown in **Figure 7 (b).** High magnification observation of the region of transition from crack initiation, which is a smooth and relatively featureless fracture surface, to early microscopic crack growth, which is distinctly a microscopically rough fracture surface, is shown in **Figure 7 (c).** The region of unstable crack growth prior to overload revealed an array of macroscopic and fine microscopic cracks as can be seen in Figure 7 (d) indicative of "locally" operating or occurring brittle failure mechanisms.

Scanning electron micrographs of the sample of stainless steel 2304 cyclically deformed at room temperature (80° F) and at a maximum stress of 486 MPa, with a resultant fatigue life of 6,600 cycles are shown in **Figure 8**. The overall morphology of failure, revealing distinct regions of: (a) crack initiation, (b) stable crack growth, and (c) overload is shown in **Figure 8 (a**). High magnification observation of the region of crack initiation revealed predominantly transgranular failure with radial propagation of the fatigue damage (**Figure 8 (b**)). At the higher allowable magnifications of the scanning electron microscope revealed an array of fine microscopic cracks intermingled with isolated macroscopic cracks as shown in **Figure 8 (c)**. In the region of stable crack growth striation-like features were observed indicative of the occurrence of localized micro-plastic deformation (**Figure 8 (d)**). The region of unstable crack growth revealed an observable population of both macroscopic and fine microscopic cracks. In this region, a coplanar array of fine microscopic cracks, indicative of 'locally' brittle failure mechanisms were evident at the higher allowable magnifications of the scanning electron microscope (SEM).

4.5.2 At elevated temperature (400 ° F)

Scanning electron micrographs of the sample of stainless steel 2304 cyclically deformed at a maximum stress of 318 MPa and a fatigue life of 48,839 cycles at 400° F is shown in **Figure 9**. The overall morphology of failure revealed distinct regions of crack initiation, early microscopic crack growth and overload as seen in **Figure 9 (a)**. High magnification observation of the region of crack initiation revealed the transgranular region to be inlaid with an array of fine microscopic cracks (**Figure 9 (b**)). The region of stable fatigue crack growth revealed fine striation-like features (**Figure 9 (c)).** This is an indication of the occurrence of "localized" micro plastic deformation. The region of overload revealed an array of coplanar macroscopic cracks as shown in **Figure 9 (d).**

High magnification observation of the region of unstable crack growth revealed an array of fine microscopic cracks.

Scanning electron micrographs of the sample of stainless steel 2304 cyclically deformed at a maximum stress of 344 MPa and a fatigue life of 11,351 cycles at 400° F is shown in **Figure 10**. The overall morphology of failure revealed distinct regions of crack initiation, early microscopic crack growth, and overload as shown in **Figure 10 (a).** High magnification observation of the region between stable microscopic crack growth and unstable crack growth as shown in **Figure 10 (b).** The region of stable crack growth when observed at the higher allowable magnifications of the SEM revealed an array of fine microscopic cracks inter-dispersed with pockets of very fine and shallow striations indicate of localized micro plastic deformation **(Figure 10 (c)).** An array of fine microscopic cracks and shallow striations were also observed in the region of stable crack growth prior to overload **(Figure 10 (d))**. These features are clearly indicative of the occurrence of both ductile and brittle failure mechanisms at the fine microscopic level.

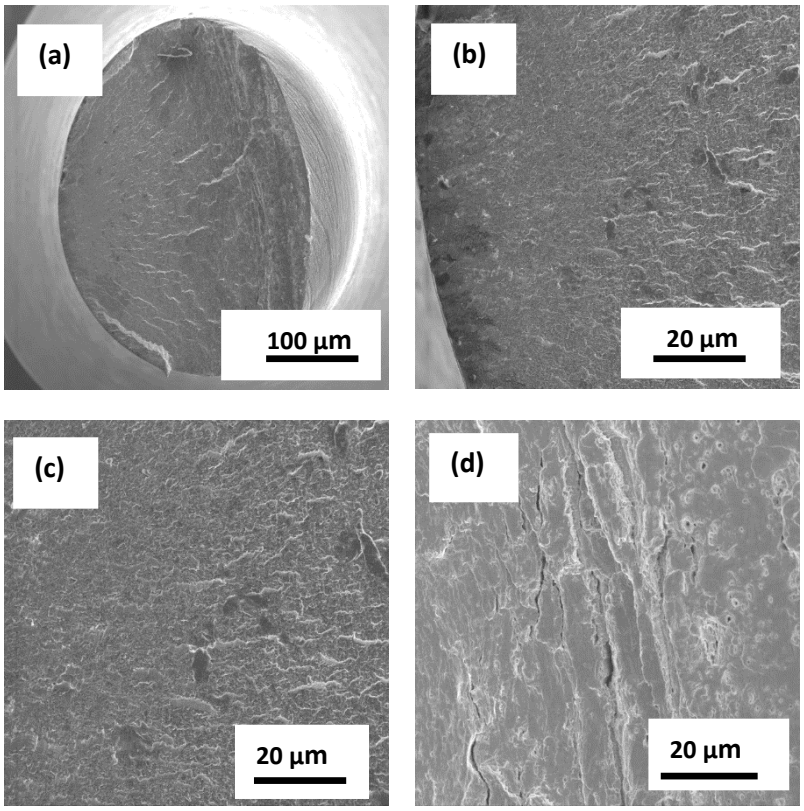

Figure 7. Scanning electron micrographs of the sample of stainless steel 2304 cyclically deformed at **room temperature (80ºF)** at a maximum stress of 389 MPa, resulting fatigue life of 96,000 cycles, showing:

(a) Overall morphology of failure revealing region of crack initiation, stable crack growth and overload.
(b) High magnification observation of the region of crack initiation.
(c) High magnification observation of (b) showing the transition from crack initiation (smooth fracture surface) to early microscopic crack growth (microscopically rough fracture surface).
(d) An array of macroscopic and fine microscopic cracks in the region of unstable crack growth prior to overload.

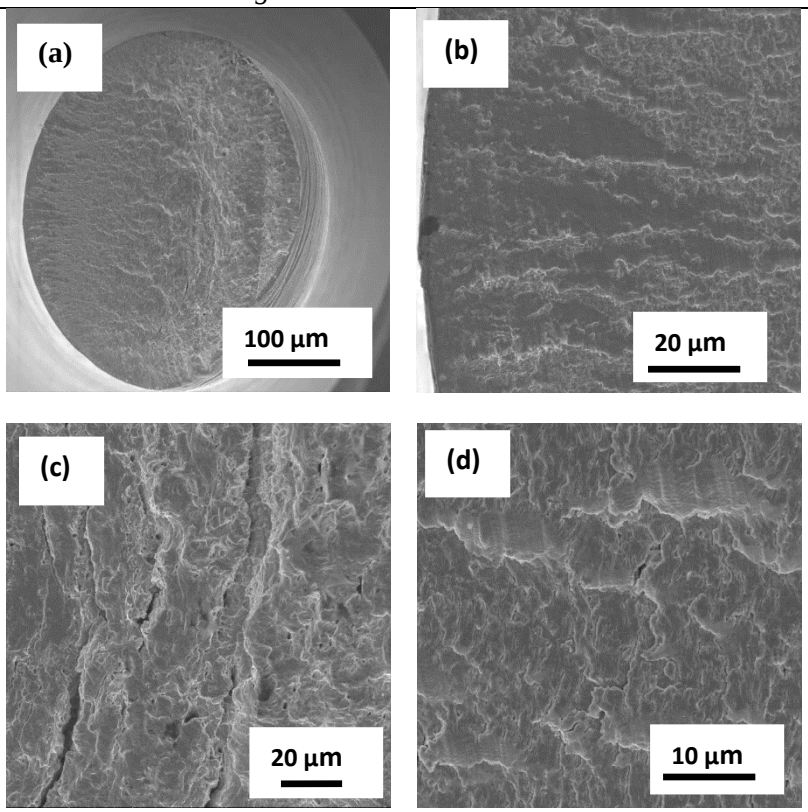

Figure 8. Scanning electron micrographs of the sample of stainless steel 2304 cyclically deformed at room temperature (27ºC) at a maximum stress of 486 MPa, with fatigue life of 6,600 cycles, showing:

(a) Overall morphology of failure showing the distinct regions of crack initiation, stable crack growth and overload.
(b) Region of crack initiation revealing transgranular failure and radial propagation of fatigue damage.
(c) High magnification observation of (b) showing an array of fine microscopic cracks
(d) Striation-like features indicative of micro-plastic deformation in the region of stable crack growth.

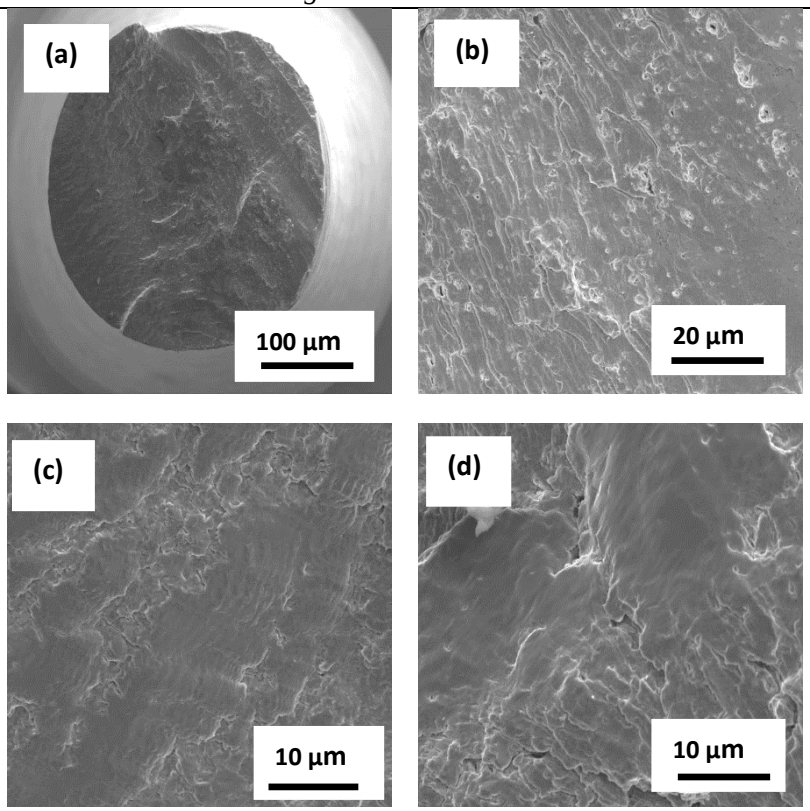

Figure 9. Scanning electron micrographs of the sample of stainless steel 2304 cyclically deformed at a maximum stress of 318 MPa and a fatigue life of 48,839 cycles at 400 F, showing:

(a) Overall morphology of failure revealing the distinct regions of crack initiation, early microscopic crack growth and overload.

(b) High magnification observation of the region of crack initiation revealing transgranular failure inlaid with fine microscopic cracks.

(c) Striation-like features indicative of localized micro plastic deformation in the region of stable crack growth.

(d) Array of coplanar macroscopic cracks region of unstable crack growth prior to overload.

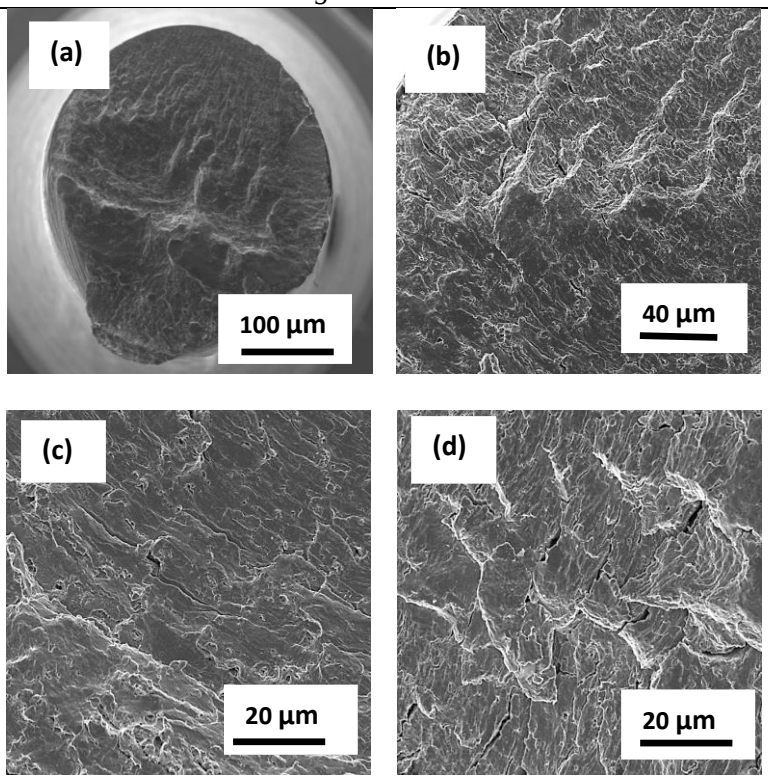

Figure 10. Scanning electron micrographs of the sample of stainless steel 2304 cyclically deformed at a maximum stress of 344 MPa and a fatigue life of 11,351 cycles at 400° F, showing:
(a) Overall morphology of failure showing the distinct regions of crack initiation, microscopic crack growth and overload.
(b) High magnification observation of the region of between stable microscopic crack growth an unstable crack growth.
(c) High magnification observation of the region of stable crack growth revealing an array of fine microscopic cracks inter-dispersed with pockets of very fine and shallow striations indicative of localized micro plastic deformation.
(d) An array of fine microscopic cracks and shallow striations in the terminal region of stable crack growth prior to overload.

5. Conclusions

Based on the results of a recent study attempting to understand the influence of microstructure on mechanical response to include hardness, tensile properties and cyclic fatigue behavior of a duplex stainless steel 2304, following are the key observations or conclusions:

1. The longitudinal (L) section revealed a mixture of light and dark regions. The light color region, or island, can be categorized to be pockets of ferrite (pure iron), while the darker, or gray color, region are a mixture of very fine pearlite and austenite. Also, the longitudinal (L) section revealed a minimal distribution of the coarse second-phase particles. The transverse (T) section of the as-provided material revealed a healthy mixture of very fine grains. The light color region, or island, represents ferrite (or pure iron), while the darker region represents a combination of pearlite and austenite.

2. The microhardness was measured and an average value of 514 kg/mm^2. Macro-hardness was measured using Rockwell 'B' scale and ranged from 68.90 kg/mm^2 to 76.63 kg/mm^2 with an average value of 74.17 kg/mm^2.

3. The elastic modulus of the chosen steel was 242 GPa at room temperature [80° F] and 222 MPa at the elevated temperature [400° F], a nine percent decrease in elastic modulus because of an increase in test

temperature. Yield strength of the stainless steel at room temperature was 648 MPa and at the elevated temperature 530 MPa; a noticeable twenty percent decrease in strength with an increase in test temperature. The ultimate tensile strength (σ_{UTS}) at room temperature (80° F) was 808 MPa and 718 MPa at the elevated temperature (400 F), an observable decrease of 11 percent due to an increase in test temperature. The ductility quantified by elongation-to-failure was 48.0 pct. at room temperature (80 ° F) and 40.0 pct. at the elevated temperature (400 ° F) revealing a decrease with an increase in test temperature.

4. Tensile fracture at both temperatures was predominantly cup and cone morphology. High magnification observation of the fracture surface revealed a healthy combination of dimples of varying size, isolated microscopic voids, and macroscopic cracks. At both temperatures, the overload fracture surface revealed a population of voids of varying size in combination with dimples, features indicative of the occurrence of "locally" dominant ductile failure mechanisms.

5. At both temperatures, i.e., room temperature (80° F) and elevated temperature (400°F) the variation of maximum stress (MPa) with fatigue life (cycles) followed the trend shown by most ferrous metals and their alloy counterparts. An increase in cyclic fatigue life with a decrease in maximum stress. At equivalent values of maximum stress, the fatigue life noticeably degraded by as much as 100 pct. at the higher test temperature.

6. At room temperature (80° F), test specimens cyclically deformed at a high value of maximum stress and resultant short fatigue life and a low value of maximum stress and resultant enhanced fatigue life the fracture surfaces revealed distinct regions of crack initiation, stable crack growth and overload.

7. At the elevated test temperature (400 ° F) test specimen of stainless steel 2304 cyclically deformed at a maximum stress of 318 MPa and a fatigue life of 48,839 cycles at 205°C revealed an overall morphology of failure to comprise of distinct regions of crack initiation, early microscopic crack growth and overload.

References

1. Dowling, N.E., "Mechanical Behavior of Materials", Prentice Hall, Upper Saddle River, New Jersey, USA, Third Edition, 2007.

2. Zhang, L., Han, Z, Zhang, Z., Guan, H and W. Ke: "The Corrosion of Stainless Steels and Nickel Base Superalloy in Subcritical Water Condition," Acta Metallurgica Sinica, Vol. 39, No. 6, 2003, pp. 649-654.

3. Online material for "Background on stainless-steels", http://www.amoz.com/article.aspx/Article ID 470.

4. Online material for the "Families of stainless steel" http://www.azom.com/article.aspx?ArticleID=470#.

5. Online material for the "Characteristics of stainless steels, http://www.azom.com/article.aspx?ArticleID=470#

6. McGurn, J.F., "Stainless Steel Reinforcing Bars in Concrete" Online material http://citeseerx.ist.psu.edu/viewdoc/download?doi=10.1.1.475.5101&rep=rep1&type=pdf

7.. ASM Materials Handbook Volume 1: Properties and Selection: Irons, Steels, and High-Performance Alloys, American Society for Materials International (ASM Int.), Materials Park, Ohio USA.

8. Dieter, G. E., Mechanical Metallurgy, McGraw Hill Publishers, New York, USA, 2000.

9. ASM Materials Handbook: Volume 4A: Steels: Heat Treating Fundamentals and Processes, American Society for Materials International (ASM Int.), Materials Park, Ohio USA.

10. ASTM E-8: "Standard Test Method for Tension Testing of Metallic Materials," American Society for Testing Materials, Philadelphia, PA, USA, 1990.

11. Thomas H. Courtney, Mechanical Behavior of Materials, Second Edition, McGraw Hill, New York, 2000.

12. Srivatsan, T.S., Manigandan, K, and Thomas Quick: "The Tensile Deformation and Fracture Behavior of Four High Strength Steels," Steel Research International, Vol. 82, Issue 12, pp. 1385-1393, 2011

13. Srivatsan, T.S., Manigandan, K., Freborg, A., and Quick, T., "Investigating and Understanding the Cyclic Fatigue, Deformation, and Fracture Behavior of a Novel High Strength Alloy Steel: Influence of Orientation" Steel Research International, Volume 84, Issue 3, pages 218–228, March 2013

14. Srivatsan, T.S., Manigandan, K., Freborg, A., and Quick, T., "The Quasi Static Deformation and Fracture Behavior of a Novel High Strength Steel for Emerging Applications," Emerging Materials Research, Vol. 2, pp. 17-26, 2013, pp. 17-26.

15. Manigandan, K., Srivatsan, T.S., Quick, T., Freborg, A.M., and Sastry, S., "The Microstructure and Mechanical Behavior of High Strength Alloy Steel X2M" Advances in Materials Research, An International Journal, Advances in Material Research, Vol. 3, No. 1 (2014) 283-295.

16. Manigandan, K., Srivatsan, T.S, Tammana, D., Behrang, P., and Vasudevan, V.K., "Influence of Microstructure on Strain-controlled Fatigue and Fracture Behavior of Ultra High Strength Alloy Steel AerMet® 100," Materials Science and Engineering, Volume 601, April 2014, Pages 29–39.

17. Gowda, S., Hotz, C., Manigandan, K., Srivatsan, T.S., Patnaik, A, and Payer, J.: "Quasi-Static, Cyclic Fatigue and Fracture Behavior of Alloy Steel for Structural Applications: Influence of Orientation", Materials Performance and Characterization, ASTM International, doi:10.1520/MPC20150030/Vol. 5/No. 1/2016/, available online at www.astm.org, March 2016, 16 pages.

18. Gowda, S, Patnaik, A., Payer, J., and Srivatsan, T.S., "Extrinsic Influence of Environment-Induced Degradation on Load Carrying Capacity of Steel Beams", Journal of Materials Engineering and Performance, available online, DOI: 10.1007/s11665-015-1725-5 Oct 1, 2015, pp. 4224-4235.

19 Gowda, S., Hotz, S., Patnaik, A., Manigandan, K., and Srivatsan, T.S: "The Microstructure, Tensile Response and Fracture Behavior of a High Performance Steel: influence of orientation, Emerging Materials Research, Volume 4, Issue EMR2, http://dx.doi.org/10.1680/emr.15.00018, Nov 19 2015, pp. 255-264.

20. Xia, N., Qingwen, R., Liang, R.Y., Payer, J and A. Patnaik: "Non-Uniform Corrosion Induced Stresses in Steel Reinforced Concrete, ASCE Journal of Engineering Mechanics, Vol. 138, No. 4, April 2012, pp. 338-346.